EMERGING ADVANCES IN INTEGRATED TECHNOLOGY
e-ISSN: 2773-5540

EmAIT

Vol. 6 No. 2 (2025) 11-26
https://publisher.uthm.edu.my/ojs/index.php/emait

Mini Review of RF Magnetron Sputtering for Aluminum Nitride Thin Film Deposition: Scale-Up Challenges and Perspectives

Natasya Salsabiila[1,2], Nafarizal Nayan[1,2]*, Zulkifli Azman[1,2], Ahmad Shuhaimi Abu Bakar[3], Sharaifah Kamariah Wan Sabli[4], Feri Adriyanto[5]

[1] *Faculty of Electrical and Electronic Engineering, Universiti Tun Hussein Onn Malaysia, 86400 Parit Raja, Batu Pahat, Johor, MALAYSIA*
[2] *Microelectronics and Nanotechnology – Shamsuddin Research Centre, Universiti Tun Hussein Onn Malaysia, 86400 Parit Raja, Batu Pahat, Johor, MALAYSIA*
[3] *Low Dimensional Material Research Centre, Universiti Malaya, 50603 Kuala Lumpur, MALAYSIA*
[4] *MIMOS Berhad, Technology Park Malaysia, 57000 Kuala Lumpur, MALAYSIA*
[5] *Department of Electrical Engineering, Universitas Sebelas Maret, 57126 Jawa Tengah, INDONESIA*

*Corresponding Author: nafa@uthm.edu.my
DOI: https://doi.org/10.30880/emait.2025.06.02.002

Article Info

Received: 29 September 2025
Accepted: 28 December 2025
Available online: 31 December 2025

Keywords

Aluminum nitride, RF magnetron sputtering, thin film

Abstract

Radio Frequency (RF) magnetron sputtering is a pivotal technique in thin-film deposition, renowned for its versatility and precision in producing high-quality crystalline films. This method excels in delivering uniform film deposition, high reproducibility, and adaptability for both insulating and conductive materials. Among the materials deposited using RF magnetron sputtering, Aluminum Nitride (AlN) has gained attention due to its wide bandgap, high thermal conductivity, and excellent breakdown voltage. Over the years, researchers have successfully deposited c-axis-oriented AlN films with thicknesses ranging from 8 nm to 2.75 µm, typically on small wafers (2–4 inches) at temperatures up to 900 °C. This mini-review explores the fundamentals, working principles, and application of RF magnetron sputtering for AlN thin film deposition. The novelty lies in synthesizing existing literature on RF magnetron sputtering for AlN deposition and systematically linking key sputtering parameters (RF power, working pressure, gas flow ratio, substrate temperature, target-to-substrate distance, and post-annealing) to film properties, while highlighting the challenges of scaling up to larger wafers. These insights offer a practical reference for optimizing AlN deposition at larger scales.

1. Introduction

Among techniques to be used in thin-film deposition, radio frequency (RF) magnetron sputtering has emerged as a reliable and versatile method, renowned for its ability to produce high-quality crystalline films with excellent control over film properties [1]. Its adaptability in depositing a broad range of materials, including both insulating and conductive targets, has made it a preferred method for researchers and industries [2]. Compared to other

deposition techniques, RF magnetron sputtering excels in providing uniform film deposition, high reproducibility, and compatibility with various substrate materials, even at relatively low substrate temperatures. These advantages make it an essential tool for applications requiring exceptional precision, such as in microelectronics, optoelectronics, and high-frequency devices [3].

RF magnetron sputtering operates by utilizing RF power to generate a plasma, which facilitates the ejection of atoms from a target material onto a substrate. This technique enables precise control over critical deposition parameters, including RF power, working pressure, gas flow ratio, substrate temperature, target-to-substrate distance, and post-annealing. These factors play a pivotal role in determining the thin film's properties, such as crystallinity, thickness, and morphology [4, 5]. Moreover, the alternating electric field in RF sputtering overcomes the issue of charge accumulation on insulating targets, a common limitation in direct current (DC) sputtering, broadening the range of materials that can be effectively deposited [6].

Among the materials that can be deposited using RF magnetron sputtering, Aluminum Nitride (AlN) is particularly attractive due to its wide bandgap, high thermal conductivity, and excellent breakdown voltage. For example, AlN thin film is widely employed as a buffer layer in Gallium Nitride (GaN)-based High Electron Mobility Transistors (HEMTs) to enhance structural integrity and mitigate lattice mismatch [7]. RF magnetron sputtering has proven to be an effective technique for depositing high-quality AlN thin film, offering precise control over deposition parameters to tailor film quality [8]. Therefore, this mini review provides an overview of RF magnetron sputtering, emphasizing its fundamental principles and targeted applications in the deposition of AlN thin film.

2. Fundamental Theory of RF Magnetron Sputtering

In a magnetron sputtering system, plasma generation is a critical process that depends on achieving electrical breakdown. Once this breakdown is reached, a stable plasma forms, facilitating efficient ion bombardment of the target material [2, 9]. The ions generated within the plasma are essential for sputtering, as they dislodge atoms from the target surface. Electrical breakdown occurs when the electric field between the electrodes exceeds a critical threshold, ionizing gas molecules to form plasma. This ionization process follows the Townsend discharge mechanism, where free electrons gain energy from the electric field, collide with neutral gas atoms, and cause further ionization, initiating a cascade effect [10]. The dynamics of this process are described by Equation 1.

$$\alpha = \frac{1}{\lambda_e} \exp\left(-E_i/\varepsilon_e\right) \tag{1}$$

where,

α : first Townsend coefficient
λ_e : mean free path of an electron
E_i : ionization threshold of the gas
ε_e : electron energy colliding with a gas atom

During the sputtering process, energetic ions bombarding the target surface can eject secondary electrons [11]. This ejection occurs through two primary mechanisms: potential electron emission (PEE), which releases electrons due to ion neutralization, and kinetic electron emission (KEE), resulting from energy transfer as ions penetrate the target material [12]. The efficiency of secondary electron emission (SEE) is quantified by the secondary electron emission coefficient, as defined in Equation 2 [13].

$$\gamma = \frac{j^-}{j^+}\Big|_{cathode} \tag{2}$$

where,

γ : secondary electron emission coefficient
j^- : current density of electrons
j^+ : current density of ion

For metallic targets, singly charged metal ions are unable to induce potential electron emission, resulting in negligible SEE during the self-sputtering process, with the SEE coefficient effectively being zero [4]. However, during AlN deposition using a metallic aluminum target, the introduction of nitrogen in the sputtering atmosphere significantly alters the surface interactions. Although the aluminum target inherently exhibits a low SEE coefficient, the reactive nitrogen environment modifies surface energy dynamics. This interaction facilitates some degree of SEE, as ionization and collisions with nitrogen ions alter the surface conditions, enabling electron release [14].

Emerging Advances in Integrated Technology Vol. 6 No. 2 (2025) p. 11-26

The relationship between breakdown voltage and gas pressure in the sputtering chamber during the deposition process is further described by Paschen's Law, as shown in Equation 3 [15]. The constants used in support of Equation 3 are listed in Table 1.

$$V_B = \frac{Bpd}{\ln(Apd) - \ln\left(\ln\left(1+\frac{1}{\gamma}\right)\right)} \tag{3}$$

where,
V_B : breakdown voltage
A and B : constants that depend on the gas type
p : gas pressure
d : distance between the electrodes
γ : secondary electron emission coefficient

Table 1 *Constants for Townsend ionization*

Gas	A ($cm^{-1}Torr^{-1}$)	B (V/cmTorr)
Air	14.6	365
H_2	5	130
Ar	13.6	235
N_2	11.8	325
He	2.8	3.4
H_2O	12.9	289
CO_2	20	466

The next essential parameter is the sputter yield, which quantifies the efficiency of material ejection from the target under energetic ion bombardment. It is defined as the number of atoms ejected from the target surface per incident ion [16, 17]. The sputter yield is also used to determine the sputter rate, as outlined in Equation 4 [4].

$$R = \frac{Y J_i}{e n_{target}} \tag{4}$$

where,
R : sputter rate
J_i : ion current density
e : electron charge
n_{target} : atomic density of the target

To enhance the lifetime of electrons escaping from the cathode and to capture them near the cathode target, magnetic fields were introduced in sputtering systems as early as 1936 [18]. Figure 1 shows a schematic of a magnetron sputtering system. In a magnetron sputtering system, the electron trajectory becomes more complex due to the combined effects of magnetic and electric fields. In the absence of an electric field, electrons spiral within the magnetic field, following a path determined by their cyclotron angular frequency and gyration radius, as outlined in Equations 5 and 6 [4].

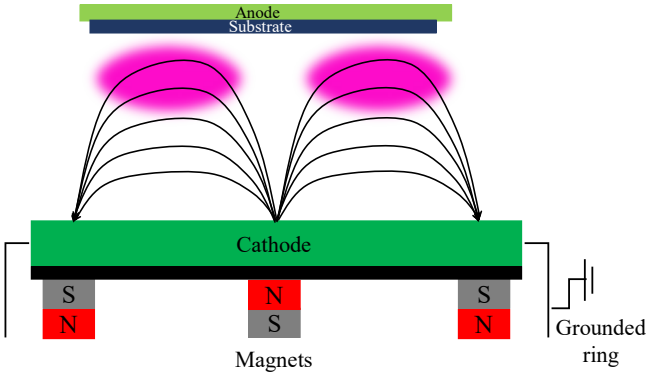

Fig. 1 *Configuration of magnetron sputtering system, redrawn from* [4] *with modifications*

$$\omega_{ce} = \frac{eB}{m_e} \tag{5}$$

where,

ω_{ce} : electron cyclotron angular frequency
e : electron charge
B : magnetic field
m_e : electron mass

$$r_{ce} = \frac{u_{e\perp}}{\omega_{ce}} = \frac{u_{e\perp} m_e}{eB} \tag{6}$$

where,

r_{ce} : gyration radius
$u_{e\perp}$: electron velocity perpendicular to the magnetic field
ω_{ce} : electron cyclotron angular frequency
m_e : electron mass
e : electron charge
B : magnetic field

3. Working Principle of RF Magnetron Sputtering

The working principle of RF magnetron sputtering involves generating plasma within a vacuum chamber by applying an RF electric field to a target material, typically positioned on a magnetron. This RF field ionizes the chamber's gas (usually argon), creating a plasma composed of ions and electrons. The electric field accelerates the ions toward the target, causing them to collide with it at high energies. These collisions dislodge atoms from the target surface, a process known as sputtering. The ejected atoms then travel through the chamber and deposit onto a substrate, forming a thin film. RF power is beneficial for sputtering insulating or reactive materials, as it enables continuous plasma generation, even when the target material is not prone to emitting electrons [5].

Figure 2 shows the common magnetic designs. In a balanced magnetron configuration, the magnetic field is symmetrically distributed around the target, promoting a uniform plasma density and ensuring a stable sputtering process. This setup optimizes the use of target material while minimizing the scattering of sputtered atoms, leading to high-quality films with excellent uniformity [1].

In contrast, unbalanced type I magnetron systems feature a magnetic field that is stronger on one side of the target, resulting in increased ionization of the sputtered material. This asymmetry enhances the deposition rate and offers better control over film properties, such as composition and microstructure. However, the increased ionization can also cause more ion bombardment on the substrate, potentially affecting the film's characteristics [19–21].

Unbalanced type II magnetron sputtering further intensifies this effect by employing a more pronounced asymmetrical magnetic field, creating a highly ionized plasma. This configuration provides greater control over the deposition process, particularly in reactive sputtering applications where film composition and stoichiometry are critical. Additionally, unbalanced type II systems excel at depositing high-quality films on complex substrate geometries, ensuring uniform deposition rates across various surface profiles [22, 23].

Emerging Advances in Integrated Technology Vol. 6 No. 2 (2025) p. 11-26

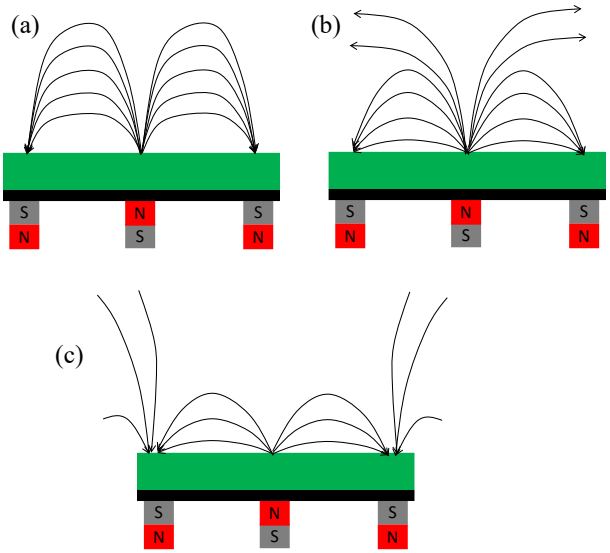

Fig. 2 *Configuration of magnetron sputtering (a) balanced; (b) unbalanced type 1; and (c) unbalanced type 2, redrawn from* [4] *with modifications*

For decades, innovations using large cylindrical targets have been central to large-area coatings. This configuration places the cathode target inside a cylindrical tube, with the magnet assembly positioned within the cylinder, as illustrated in Figure 3. One significant benefit of rotating magnetrons is their improved target utilization, achieving efficiency levels of 80-90% compared to stationary magnetrons [24–26]. Additionally, rotating magnetrons enhance the uniformity of the deposited film across larger substrates, making them highly beneficial for industrial-scale thin film deposition. This is particularly useful in applications such as solar cells, architectural glass coatings, and semiconductor devices [27].

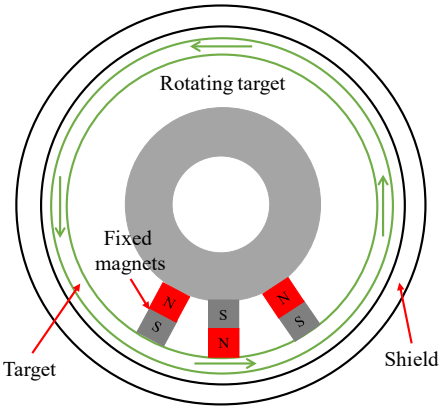

Fig. 3 *Rotating magnetron sputtering configuration, redrawn from* [4] *with modifications*

4. RF Magnetron Sputtering for Aluminum Nitride Deposition

Figure 4 illustrates the RF magnetron sputtering system used for AlN thin film deposition. The important parameters influencing the preferred AlN properties are RF power, working pressure, gas flow ratio, substrate temperature, target-to-substrate distance, and post-annealing. For instance, working pressure is related to the mean free path: a lower working pressure increases the mean free path, allowing higher-energy aluminum and nitrogen species to reach the substrate and typically promote c-axis orientation. In contrast, higher working pressure or a relatively large target-to-substrate distance compared to the mean free path reduces the arriving species' energy, which may lead to non-c-axis orientations such as a-axis [28, 29].

Figure 5 shows an example of the AlN thin film deposited using RF magnetron sputtering from a previous study. Atomic Force Microscopy (AFM) analysis revealed that the film exhibited a root mean square (RMS) surface roughness of 13.17 nm. The X-ray Diffraction (XRD) pattern confirmed that the AlN film had a strong (002) orientation. X-ray Photoelectron Spectroscopy (XPS) further indicated the presence of O 1s and C 1s peaks at ~532 eV and ~285 eV, respectively, suggesting surface contamination. To achieve the (002) orientation, the study employed a N_2 flow rate of 20 sscm, an RF power of 500 W, and a substrate temperature of 600 °C, using a relatively small Al target of 3 inches in diameter. This AlN 002 is further used as a buffer layer for GaN deposition,

resulting in high-quality GaN (002) with FWHM of 1.03^0, increasing quality from 3.99^0 without AlN [30]. Hence, RF magnetron sputtering for depositing high-quality AlN thin film is very promising.

Table 3 further summarizes other studies utilizing RF magnetron sputtering for AlN thin film deposition. This data shows that highly c-axis-oriented AlN can be achieved on a wide range of substrates across a broad temperature window from room temperature up to approximately 900 ^{0}C. The reported films also vary significantly, ranging from ultrathin layers of around 8 nm to thick films exceeding 2.75 µm, depending on deposition conditions. Despite these advances, most studies remain limited to small wafer sizes, such as 2 – 4 inches.

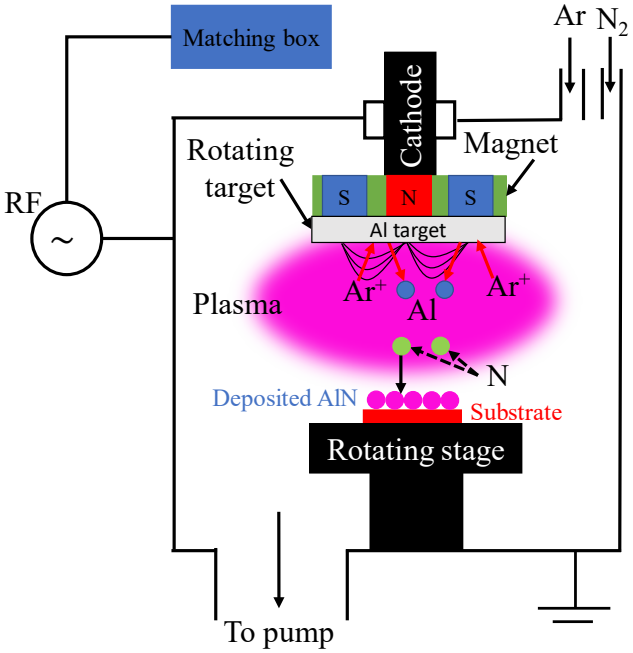

Fig. 4 *AlN deposition process using RF magnetron sputtering, redrawn from* [31] *with modifications*

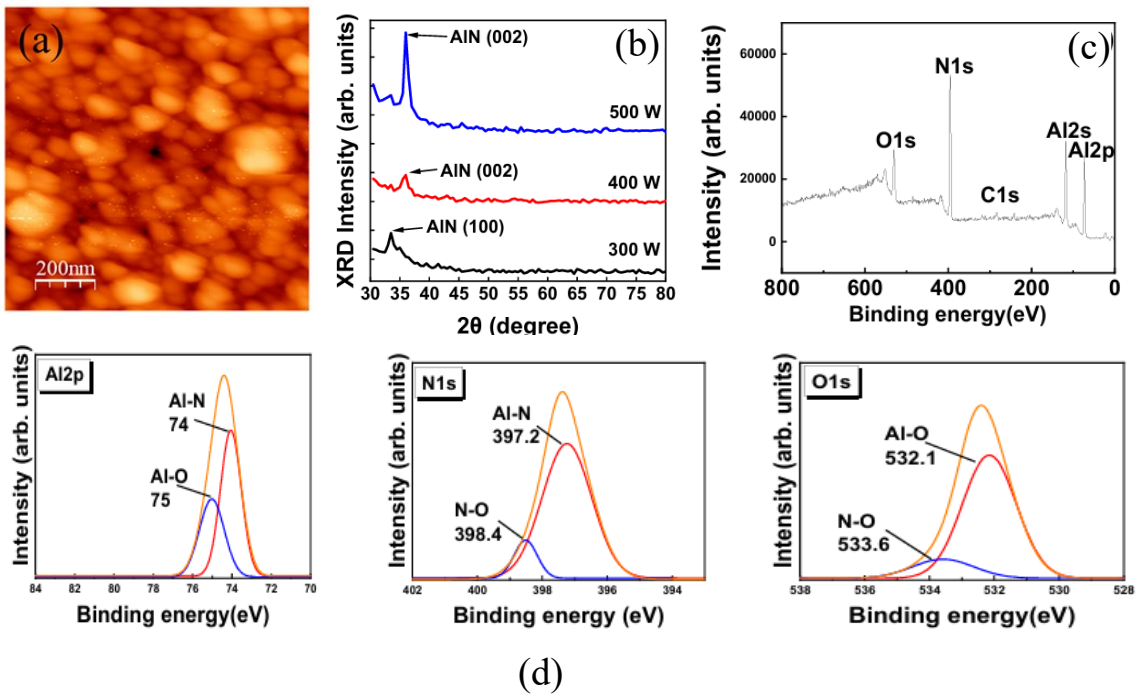

Fig. 5 *(a) AFM; (b) XRD; (c) XPS survey spectrum; and (d) XPS core level for AlN deposited by RF magnetron sputtering technique, adapted from* [30]*, open access under the Creative Commons Attribution license*

Emerging Advances in Integrated Technology Vol. 6 No. 2 (2025) p. 11-26

5. Scale-up Challenge Perspectives

RF magnetron sputtering is a highly effective technique for producing c-axis-oriented AlN films, which are critical for various applications. Recent research has predominantly utilized RF magnetron sputtering systems with small target diameters, typically around 3 inches, primarily designed for academic studies. While this setup has proven effective for depositing AlN films mostly on wafers 2 – 4 inches, as shown in Table 3, it falls short when addressing the needs of industrial applications. To meet industrial-scale requirements, a shift toward larger wafer sizes, such as 8 inches or more, is essential [32]. This transition requires magnetron systems with larger targets (typically around 12 inches) and appropriately redesigned vacuum chambers.

A key challenge in scaling up is maintaining uniform AlN deposition across the entire wafer. Achieving consistent film thickness and crystalline orientation on 8-inch wafers is more difficult, as sputtering rates, gas distribution, and ion flux can vary across the substrate. Such variations can negatively affect device performance and reliability [33]. Optimizing deposition parameters is therefore essential. Strategies include adjusting RF power density, improving argon–nitrogen gas distribution (for example, using multi-zone gas inlets), tuning the working pressure and target-to-substrate distance, and applying variable rotation speeds to both the target and substrate. For instance, many reports indicate that academic systems typically operate at a few hundred watts for 3-inch targets, and 12-inch targets require proportionally higher RF power to maintain uniform plasma density across the erosion racetrack [34, 35]. Further relation between each sputtering parameter on the deposited AlN film is shown in Figure 6, observed from the existing literature listed in Table 2. This relationship can be used as a reference for large wafer transition using a large target size.

Scaling up also changes chamber dynamics. As the target and chamber size increase, plasma behavior becomes more complex, potentially causing variations in the energy and trajectory of sputtered species [36]. Addressing these issues requires a detailed investigation into how chamber size influences plasma stability, ion bombardment uniformity, and target erosion patterns. Advanced simulation techniques, including computational fluid dynamics (CFD) and plasma modeling, offer powerful tools to analyze these dynamics and provide actionable insights for optimizing sputtering system design. Experimental diagnostics, particularly optical emission spectroscopy (OES) and Langmuir probes, are essential for validating plasma behavior. While previous studies have mainly focused on these diagnostics in small chambers [37–39], there is a clear gap in the literature for large-area systems, making such investigations particularly valuable.

Table 2 *Overview of AlN thin film deposition using RF magnetron sputtering*

Year	Author	Substrate	Size	Temperature	Plane direction	Thickness	Deposition Parameter
2014	Shih *et al.* [40]	Si(100)	2”	200 ^{0}C	(002), (100)	1.76 µm	The optimum condition is using a gas ratio (N_2/Ar + N_2) of 40%, RF power 400 W, and working pressure 4mTorr. RMS value was measured at 1.9 nm. The device was used for surface acoustic wave application, with the phase velocity reaching 4,996 m/s.
2015	Kumada *et al.* [41]	Nitride sapphire	2”	823, 873, and 923 ^{0}K	(002)	1.6 µm	The growth rate is 2.4 µm/h (RF power: 900 W) and 2.9 µm/h (RF power: 1,000 W). The edge-type dislocation density is estimated at 10^{10} cm^{-2}, and the screw and mixed dislocation density is estimated at 10^9 cm^{-2}.
2015	Mori *et al.* [42]	Si(100)	-	200 – 400 ^{0}C	(002), (101)	120 nm	The optimum parameter is 35% N_2, working pressure of 2 mTorr, and RF power of 250 W, resulting growth rate of 2 nm/min. RMS value was 15 nm.

Year	Author	Substrate	Size	Temperature	Plane direction	Thickness	Deposition Parameter
2016	Kang *et al.* [43]	Patterned sapphire substrate	-	500 ^{0}C	(002)	200 nm	The optimum RF power used was 500 W, with an RMS value was 8.278 nm.
2016	Miyake *et al.* [44]	*c*-plane sapphire	2"	650 ^{0}C	(002), (1012)	170 – 340 nm	The post-annealing temperature used is 1,600 – 1,700 ^{0}C for 1 hour. The RF power used was 700 W, and an Ar/N_2 ratio of 0.33. The roughness varied from 0.40 nm to 0.91 nm.
2017	Jinno *et al.* [45]	*c*-plane sapphire	-	Room temperature, 300 and 600 ^{0}C	(002), (1120)	30 nm	The RF power used was 450 W, with the Ar and N_2 flow rates used was 5 standard cc/min. The annealing process was conducted at 1,600 ^{0}C. The RMS value increased from 0.18 nm to 2.47 nm.
2017	Jeong *et al.* [46]	*c*-plane sapphire	2"	700 ^{0}C	(002)	30 nm	The RF power used was 300 W, with an N_2 flow was 90 sscm. The RMS value was 0.270 – 1.828 nm.
2018	Cascajero *et al.* [47]	p-Si(111)	2"	450 ^{0}C	(002)	8 – 25 nm	The variation of RF power used was 150 – 225 W. The roughness was below 1.7 nm.
2018	Chen *et al.* [48]	Diamond(111)	-	400 ^{0}C	(002), (100)	1.2 µm	The parameter used was the variation of total pressure in the reactor (0.2 – 0.6 Pa) and Ar/N_2 ratio (3:1, 5:2, 2:1, 5:3, and 3:2). The sample rotation used was 30 r/min. The RF power used was 250 W. The electromechanical coupling coefficient was 6.2 %, with the resistivity was 2.88×10^{12} Ωcm.
2018	Hakamata *et al.* [49]	*c*-plane sapphire	-	650 ^{0}C	(002), (1012)	200 nm	The thin film was annealed at 1,700 ^{0}C for 3 hours in an N_2 atmosphere. The RF power used was fixed at 700 W. The full width at half maximum (FWHM) value was 97 – 214 arcsec.
2019	Huang *et al.* [50]	*c*-plane sapphire	-	650 ^{0}C	(002), (1012)	50 nm	RF power used was 750 W. The parameters used were annealing time (0 – 6 hours) and annealing temperature (1,450 – 1,550 ^{0}C). The FWHM values for (002) and (1012) were 28 and 410 arcsec, respectively.

Emerging Advances in Integrated Technology Vol. 6 No. 2 (2025) p. 11-26

Year	Author	Substrate	Size	Temperature	Plane direction	Thickness	Deposition Parameter
2019	Ke *et al.* [51]	Sapphire	2”	550 ^{0}C	-	-	The AlN film layer was deposited through the hybrid method. The N_2 flow rate was 1.4 sscm, with an RF value of 50 W. The leakage current density was 4.38 × $10^{-6} A/cm^2$.
2019	Ishimoto *et al.* [52, 53]	*c*-plane sapphire	2”	600 ^{0}C	(002), (102)	20 nm	The RF power used was 450 W. The piezoelectric field was varied from 3.48 to 3.72 MV/cm, with an efficiency drop of 4 – 13 %.
2019	Ge *et al.* [54]	*c*-plane sapphire	-	200 ^{0}C	(002)	2.75 µm	The RF power used was 300 W, with working pressure at 0.8 Pa, Ar:N_2 ratio of 1:3, and sputtering time varied from 60 to 120 minutes. The surface roughness is as low as 2.012 nm, and the resistivity reached 4.36×10^{12} Ωcm.
2020	Song *et al.* [55]	Sapphire(002)	2”	460 – 610 ^{0}C at 30^0 interval	(002), (1011)	700 nm	The FWHM value was 2,455.2 arcsec for the (002) plane and 3,992.4 arcsec for the (1011) direction.
2020	Zeng *et al.* [56]	Sapphire	-	550 ^{0}C	-	25 nm	The RF power used was fixed at 50 W, with the background pressure fixed at 10-^{7} Torr.
2020	Feng *et al.* [57]	*c*-plane sapphire	2”	650, 800, and 900 ^{0}C	(1122)	500 nm	The working pressure was kept at 5 mTorr, with the annealing process conducted at 1,600 ^{0}C for 4 hours in a 150 Torr N_2 atmosphere. The surface roughness varied from 0.376 nm to 5.433 nm. The optimum deposition temperature was 800 ^{0}C, with the threading dislocation density was $7.5 \times 10^9 cm^{-2}$.
2020	Bakri *et al.* [58]	Si(100)	2”	Room temperature	polycrystalline	199.85 nm	The Ar and N_2 gases used were 100 sscm and 50 sscm, respectively. The working pressure was set at 5 mTorr, and the RF power was 200 W.

Year	Author	Substrate	Size	Temperature	Plane direction	Thickness	Deposition Parameter
2020	Gu *et al.* [59]	*c*-plane sapphire	2”	550 – 770 ^{0}C	(002), (1012)	200 nm	The RF power was set at 2,000 and 3,000 W, with the N_2 gas flow being 100 – 180 sscm. The post-annealing treatment was performed at 1,700 ^{0}C for 3 hours. The RMS value increased from 1.51 to 1.93 nm.
2021	Li *et al.* [60]	*c*-plane sapphire	2”	650 ^{0}C	(002), (1012)	25 nm	The annealing temperature used was 1,500 ^{0}C in the H_2 and N_2 mixture atmosphere for 30 minutes. The N_2 gas flow rate used was 200 sscm, with fixed RF power at 750 W.
2021	Uesugi *et al.* [61]	*c*-plane sapphire	2”	600 ^{0}C	(002), (004), (006)	300 nm	The RF power is set at 700 W. The RMS value was measured at less than 0.25 nm. The dislocation found was a screw type and mixed-type.
2021	Shojiki *et al.* [62]	*c*-plane sapphire	-	-	(002), (1012)	190 nm	The FWHM value for the (002) plane was 15 arcsec, and for the (1012) plane was 280 arcsec.
2022	Peng *et al.* [63, 64]	Sapphire	2”	350 ^{0}C	(100), (110)	-	The deposition time was 1 hour, working pressure at 0.5 Pa, N_2 flow rate of 1 – 6 sscm, and RF power of 100 W. The band gap energy varied from 4.48 to 5.58 eV.
2022	Liu *et al.* [30]	p-Si(111)	-	400 – 800 ^{0}C	(002), (100)	450 nm	The working pressure was maintained at 3 mTorr, with substrate rotation of 10 rpm. The RF power was varied from 300 to 500 W. Another parameter was the N_2 flow rate ratio from 50 to 100 %. The RMS value was decreased from 13.17 nm to 2.57 nm as the N_2 flow rate increased.
2023	Ueoka *et al.* [65]	Si(100) and Si(111)	-	-	(002), (1012)	-	The power used was 200 W under a 0.3 Pa mixture of N_2 and Ar atmosphere.
2024	Liu *et al.* [66]	p-Si(111)	-	-	-	150 nm	The photoluminescence was performed at 100^0 K with an emission peak at 3.37 eV (367 nm).

Emerging Advances in Integrated Technology Vol. 6 No. 2 (2025) p. 11-26

Year	Author	Substrate	Size	Temperature	Plane direction	Thickness	Deposition Parameter
2024	Azman *et al.* [67]	Si(100)	4”	-	(002)	177.87 – 191.6 nm	The dominant (002) peak was obtained near the target source. The RF power used is 300 W with a background pressure of 1×10^{-6} Torr and working pressure of 3 mTorr.

Sputtering Parameter	Crystallinity (High intensity, low FWHM)	Grain Size	Roughness	Deposition Rate	Stress	Density	Remark
Increase in RF power	▲	▲	▲	▲	▲	▲	Excessive power causes oversputtering and rough surface.
Decrease in working pressure	▲	▲	▼	▲	▲	▲	Increased mean free path enhances adatom mobility.
Medium N_2 flow ratio	▲	▲	–	▼	–	▲	Maximum 40 – 50%. Too high N_2 causes target poisoning and reduces rate.
Increase in substrate temperature	▲	▲	▼	–	▼	▲	At least 200 °C. Higher mobility enhances crystal alignment.
Decrease in target-to-substrate distance	▲	▲	▲	▲	▲	▲	Higher arrival energy; too close affects bombardment-induced stress.
Post annealing	▲	▲	▼	–	▼	▲	Typically 600–1100 °C, some studies use up to 1600 °C.

	Increase
	Slightly increase
	Neutral/not related
	Slightly decrease
	Decrease

Fig. 6 *Relationship of magnetron sputtering parameters on the properties of AlN thin film*

6. Conclusion

This mini review highlights the fundamental theory of RF magnetron sputtering, its working principle, and its application for AlN thin film deposition. Researchers have deposited AlN (002) films ranging from 8 nm to 2.75 µm, mostly on small wafers of 2 – 4 inches and at high temperatures up to 900 °C. The main challenge is scaling up wafer sizes and chamber systems to meet industrial demands. The mini review highlights the critical relationship of sputtering parameters, including RF power, working pressure, gas flow ratio, substrate temperature, target-to-substrate distance, and post-annealing, that affect film properties such as crystallinity, grain size, roughness, deposition rate, stress, and density of AlN films. To further support scale-up, advanced simulation approaches and experimental diagnostics are suggested to understand plasma behavior in larger chamber configurations. Overall, these insights serve as a practical reference for optimizing AlN deposition at industrially relevant scales.

Acknowledgement

This work has been supported by the Malaysia Ministry of Science, Technology and Innovation (MOSTI) under the project "High Efficiency High Electron Mobility Transistor (HEMT) for Power Electronics Modules"(MOSTI005-2021SRF/SRF-APP PG1-P3). The project was a collaborative effort between Universiti Tun Hussein Onn Malaysia, Universiti Malaya, and MIMOS Berhad.

Conflict of Interest

Authors declare that there is no conflict of interest regarding the publication of the paper.

Author Contribution

The authors confirm contributions to the paper as follows: ***manuscript preparation:*** *Natasya Salsabiila;* ***data validation:*** *Nafarizal Nayan;* ***manuscript review and editing:*** *Zulkifli Azman, Ahmad Shuhaimi Abu Bakar, Sharaifah Kamariah Wan Sabli, and Feri Adriyanto. All authors reviewed the results and approved the final version of the manuscript.*

References

[1] Kosari Mehr, A., & Kosari Mehr, A. (2023). Magnetron sputtering issues concerning growth of magnetic films: A technical approach to background, solutions, and outlook. *Applied Physics A*, *129*(9), 662. https://doi.org/10.1007/s00339-023-06945-y.

[2] Gudmundsson, J. T. (2020). Physics and technology of magnetron sputtering discharges. *Plasma Sources Science and Technology*, *29*(11), 113001. https://doi.org/10.1088/1361-6595/abb7bd.

[3] Garg, R., Gonuguntla, S., Sk, S., Iqbal, M. S., Dada, A. O., Pal, U., & Ahmadipour, M. (2024). Sputtering thin films: Materials, applications, challenges and future directions. *Advances in Colloid and Interface Science*, *330*, 103203. https://doi.org/10.1016/j.cis.2024.103203.

[4] Gudmundsson, J. T., & Lundin, D. (2020). *1 - Introduction to magnetron sputtering* (D. Lundin, T. Minea, & J. T. B. T.-H. P. I. M. S. Gudmundsson (eds.); pp. 1–48). Elsevier. https://doi.org/10.1016/B978-0-12-812454-3.00006-1.

[5] Shi, F. (2018). Introductory chapter: Basic theory of magnetron sputtering. In D. F. Shi (Ed.), *Magnetron Sputtering* (p. Ch. 4). IntechOpen. https://doi.org/10.5772/intechopen.80550.

[6] Zheng, B., Fu, Y., Wang, K., Schuelke, T., & Fan, Q. H. (2021). Electron dynamics in radio frequency magnetron sputtering argon discharges with a dielectric target. *Plasma Sources Science and Technology*, *30*(3), 35019. https://doi.org/10.1088/1361-6595/abe9f9.

[7] Yang, H., Sun, J., Wang, H., Li, H., & Yang, B. (2024). A review of oriented wurtzite-structure aluminum nitride films. *Journal of Alloys and Compounds*, *989*, 174330. https://doi.org/10.1016/j.jallcom.2024.174330.

[8] Das, A., Rath, M., Nair, D. R., Ramachandra Rao, M. S., & DasGupta, A. (2021). Realization of preferential (100) oriented AlN thin films on Mo coated Si substrate using reactive RF magnetron sputtering. *Applied Surface Science*, *550*, 149308. https://doi.org/10.1016/j.apsusc.2021.149308.

[9] Fang, D., & Marcus, R. K. (1993). *Fundamental Plasma Processes BT - Glow Discharge Spectroscopies* (R. K. Marcus (ed.); pp. 17–66). Springer US. https://doi.org/10.1007/978-1-4899-2394-3_2.

[10] Naumov, N. Y. (2015). The diffusion-ionization mechanism of the transverse propagation of Townsend and glow discharges and its influence on the stability and nature of a normal current density. *High Temperature*, *53*(3), 319–328. https://doi.org/10.1134/S0018151X15020194.

[11] Ghazal, H., & Sohail, N. (2022). *Sputtering deposition* (D. Yang (ed.); p. Ch. 2). IntechOpen. https://doi.org/10.5772/intechopen.107353.

[12] Buschhaus, R., & von Keudell, A. (2023). Secondary electron emission from magnetron targets. *Plasma Sources Science and Technology*, *32*(6), 65007. https://doi.org/10.1088/1361-6595/acd57e.

[13] Donkó, Z. (2001). Apparent secondary-electron emission coefficient and the voltage-current characteristics of argon glow discharges. *Physical Review E*, *64*(2), 26401.

[14] Wang, Y., Xia, Z., Wu, S., & Li, J. (2024). Effects of sputtering pressure on microstructure and secondary electron emission properties of AlN film prepared by magnetron sputtering. *Materials Letters*, *377*, 137319. https://doi.org/10.1016/j.matlet.2024.137319.

[15] Fu, Y., Zhang, P., Verboncoeur, J. P., & Wang, X. (2020). Electrical breakdown from macro to micro/nano scales: A tutorial and a review of the state of the art. *Plasma Research Express*, *2*(1), 13001.

[16] Rauschenbach, B. (2022). *Sputtering BT - Low-energy ion irradiation of materials: Fundamentals and application* (B. Rauschenbach (ed.); pp. 123–174). Springer International Publishing. https://doi.org/10.1007/978-3-030-97277-6_5.

[17] He, Z., Miao, L., Zhu, Z., Liang, F., Song, J., Wang, N., & Hou, X. (2023). Analysis of sputtering yield measurements for ion thruster grid materials. *AIAA Journal*, *61*(7), 2799–2809. https://doi.org/10.2514/1.J062331.

[18] Stan, G. E., Montazerian, M., Shearer, A., Stuart, B. W., Baino, F., Mauro, J. C., & Ferreira, J. M. F. (2024). Critical advances in the field of magnetron sputtered bioactive glass thin-films: An analytical review. *Applied Surface Science*, *646*, 158760. https://doi.org/10.1016/j.apsusc.2023.158760.

[19] Oberberg, M., Berger, B., Buschheuer, M., Engel, D., Wölfel, C., Eremin, D., Lunze, J., Brinkmann, R. P., Awakowicz, P., & Schulze, J. (2020). The magnetic asymmetry effect in geometrically asymmetric capacitively coupled radio frequency discharges operated in Ar/O_2. *Plasma Sources Science and Technology*, *29*(7), 75013. https://doi.org/10.1088/1361-6595/ab9b31.

[20] Tiron, V., Velicu, I.-L., Vasilovici, O., & Popa, G. (2015). Optimization of deposition rate in HiPIMS by controlling the peak target current. *Journal of Physics D: Applied Physics*, *48*(49), 495204. https://doi.org/10.1088/0022-3727/48/49/495204.

[21] Huan, J., Wu, Z., Wang, Q., Zhang, S., & Kwon, S.-H. (2023). A comparative investigation on the microstructure and thermal resistance of W-film sensor using DC magnetron sputtering and high-power pulsed magnetron sputtering. In *Magnetochemistry* (Vol. 9, Issue 4). https://doi.org/10.3390/magnetochemistry9040097.

[22] Kapran, A., Antunes, V. G., Hubička, Z., Ballage, C., & Minea, T. (2022). Investigation of the magnetron balancing effect on the ionized flux fraction and deposition rate of sputtered titanium species for the high-power impulse magnetron sputtering pulses of different lengths. *Journal of Vacuum Science & Technology A*, *41*(1), 13003. https://doi.org/10.1116/6.0002309.

[23] Li, J., Ren, G.-K., Chen, J., Chen, X., Wu, W., Liu, Y., Chen, X., Song, J., Lin, Y.-H., & Shi, Y. (2022). Facilitating complex thin film deposition by using magnetron sputtering: A review. *JOM*, *74*(8), 3069–3081. https://doi.org/10.1007/s11837-022-05294-0.

[24] Iseki, T. (2006). Flat erosion magnetron sputtering with a moving unbalanced magnet. *Vacuum*, *80*(7), 662–666. https://doi.org/10.1016/j.vacuum.2005.11.019.

[25] Iseki, T. (2009). Target utilization of planar magnetron sputtering using a rotating tilted unbalanced yoke magnet. *Vacuum*, *84*(2), 339–347. https://doi.org/10.1016/j.vacuum.2009.07.010.

[26] Goto, T., Matsuoka, T., & Ohmi, T. (2009). Rotation magnet sputtering: Damage-free novel magnetron sputtering using rotating helical magnet with very high target utilization. *Journal of Vacuum Science & Technology A*, *27*(4), 653–659. https://doi.org/10.1116/1.3139903.

[27] Berishvili, Z., Gadakhabadze, I., Dekanozishvili, G., Kipiani, M., Kordzakhia, I., & Skhiladze, G. (2023). Research and development of an innovative planar-rotational magnetron sputtering device for obtaining advanced materials. *Bull. Georg. Natl. Acad. Sci*, *17*(2).

[28] Iriarte, G. F., Rodriguez, J. G., & Calle, F. (2011). Effect of substrate–target distance and sputtering pressure in the synthesis of AlN thin films. *Microsystem Technologies*, *17*(3), 381–386. https://doi.org/10.1007/s00542-010-1198-2.

[29] Sandager, M. K., Kjelde, C., & Popok, V. (2022). Growth of thin AlN films on Si wafers by reactive magnetron sputtering: Role of processing pressure, magnetron power and nitrogen/argon gas flow ratio. In *Crystals* (Vol. 12, Issue 10). https://doi.org/10.3390/cryst12101379.

[30] Liu, W.-S., Gururajan, B., Wu, S.-H., Huang, L.-C., Chi, C.-K., Jiang, Y.-L., & Kuo, H.-C. (2022). Optimal growth conditions for forming c-axis (002) aluminum nitride thin films as a buffer layer for hexagonal gallium nitride thin films produced with in situ continual radio frequency sputtering. *Micromachines*, *13*(9), 1546. https://doi.org/10.3390/mi13091546.

[31] Iqbal, A., Walker, G., Hold, L., Fernandes, A., Lacopi, A., & Mohd-Yasin, F. (2020). Sputtering of aluminium nitride (002) film on cubic silicon carbide on silicon (100) substrate: influences of substrate temperature and deposition power. *Journal of Materials Science: Materials in Electronics*, *31*(1), 239–248. https://doi.org/10.1007/s10854-019-02480-w.

[32] Ruberti, M. (2023). The chip manufacturing industry: Environmental impacts and eco-efficiency analysis. *Science of The Total Environment*, *858*, 159873. https://doi.org/10.1016/j.scitotenv.2022.159873.

[33] Peng, X., Matthews, A., & Xue, S. (2011). Plasma-based processes and thin film equipment for nano-scale device fabrication. *Journal of Materials Science*, *46*(1), 1–37. https://doi.org/10.1007/s10853-010-4974-6.

[34] Asgary, S., Vaghri, E., Daemi, M., Esmaili, P., Ramezani, A. H., Memon, S., & Hoseinzadeh, S. (2021). Magnetron sputtering technique for analyzing the influence of RF sputtering power on microstructural surface morphology of aluminum thin films deposited on SiO_2/Si substrates. *Applied Physics A*, *127*(10), 752. https://doi.org/10.1007/s00339-021-04892-0.

[35] Zai, M.-I., Lalau, I., Manica, M., Chiriacescu, L., Antohe, V.-A., Gheorghiu, C. C., Iftimie, S., Toma, O., Suchea, M. P., & Antohe, Ştefan. (2025). Morphological and functional evolution of amorphous AlN thin films deposited by RF-magnetron sputtering. In *Surfaces* (Vol. 8, Issue 3). https://doi.org/10.3390/surfaces8030051.

[36] Rauf, S., Bera, K., Kenney, J., & Kothnur, P. (2023). Modeling of plasma processing reactors: review and perspective. *Journal of Micro/Nanopatterning, Materials, and Metrology*, *22*(4), 41503.

[37] Acosta, J., Rojo, A., Salas, O., & Oseguera, J. (2007). Process monitoring during AlN deposition by reactive magnetron sputtering. *Surface and Coatings Technology*, *201*(18), 7992–7999. https://doi.org/https://doi.org/10.1016/j.surfcoat.2007.03.048.

[38] Lu, T.-Y., Yang, Y.-P., Lo, H.-H., Wang, P. J., Lai, W., Fuh, Y.-K., & Li, T. T. (2021). Minimizing film residual stress with in situ OES big data using principal component analysis of deposited AlN films by pulsed DC reactive sputtering. *The International Journal of Advanced Manufacturing Technology*, *114*(7), 1975–1990. https://doi.org/10.1007/s00170-021-07003-8.

[39] Chen, W.-L., Zhou, W.-Y., Yuan, N.-H., Yang, S.-S., Wang, P. J., Lo, H.-H., Li, T. T., & Fuh, Y. (2023). A multi-step deposited AlN films in a DC pulsed sputtering and film characteristics classification with principal component analysis of OES data. *The International Journal of Advanced Manufacturing Technology*, *127*(5), 2955–2967. https://doi.org/10.1007/s00170-023-11694-6.

[40] Shih, W.-C., & Zoh, Z.-X. (2014). Fabrication of AlN films by RF magnetron sputtering for surface acoustic wave applications. *Ferroelectrics*, *459*(1), 52–62. https://doi.org/10.1080/00150193.2013.837768.

[41] Kumada, T., Ohtsuka, M., & Fukuyama, H. (2015). Influence of substrate temperature on the crystalline quality of AlN layers deposited by RF reactive magnetron sputtering. *AIP Advances*, *5*(1), 17136. https://doi.org/10.1063/1.4906796.

[42] Mori, T. J. A., Della Pace, R. D., de Andrade, A. M. H., Corrêa, M. A., Stamenov, P., Schelp, L. F., & Dorneles, L. S. (2015). Growth of c-axis-oriented aluminum nitride thin films onto different substrates and buffer layers. *Surface and Interface Analysis*, *47*(4), 447–453. https://doi.org/10.1002/sia.5732.

[43] Kang, B. H., Lee, J. E., Kim, D.-S., Bae, S., Jung, S., Park, J., Jhin, J., & Byun, D. (2016). Effect of amorphous and crystalline AlN buffer layers deposited on patterned sapphire substrate on GaN film quality. *Journal of Nanoscience and Nanotechnology*, *16*(11), 11563–11568. https://doi.org/10.1166/jnn.2016.13552.

[44] Miyake, H., Lin, C.-H., Tokoro, K., & Hiramatsu, K. (2016). Preparation of high-quality AlN on sapphire by high-temperature face-to-face annealing. *Journal of Crystal Growth*, *456*, 155–159. https://doi.org/10.1016/j.jcrysgro.2016.08.028.

[45] Jinno, D., Otsuki, S., Niimi, T., Sugimori, S., Daicho, H., Iwaya, M., Takeuchi, T., Kamiyama, S., & Akasaki, I. (2017). Annealing of the sputtered AlN buffer layer on r-plane sapphire and its effect on a-plane GaN crystalline quality. *Physica Status Solidi (B)*, *254*(8), 1600723. https://doi.org/10.1002/pssb.201600723.

[46] Jeong, W. S., Kim, D.-S., Cho, S. H., Kim, C., Jhin, J., & Byun, D. (2017). Surface analysis of plasma pretreated sapphire substrate for aluminum nitride buffer layer. *Korean Journal of Materials Research*, *27*(12), 699–704. https://doi.org/10.3740/MRSK.2017.27.12.699.

[47] Núñez-Cascajero, A., Valdueza-Felip, S., Blasco, R., de la Mata, M., Molina, S. I., González-Herráez, M., Monroy, E., & Naranjo, F. B. (2018). Quality improvement of AlInN/p-Si heterojunctions with AlN buffer layer deposited by RF-sputtering. *Journal of Alloys and Compounds*, *769*, 824–830. https://doi.org/10.1016/j.jallcom.2018.08.059.

[48] Chen, L., Liu, H., Liu, S., Li, C., Wang, Y., An, K., Hua, C., Liu, J., Wei, J., Hei, L., & Lv, F. (2018). Growth of high quality AlN films on CVD diamond by RF reactive magnetron sputtering. *Applied Surface Science*, *431*, 152–159. https://doi.org/10.1016/j.apsusc.2017.09.036.

[49] Hakamata, J., Kawase, Y., Dong, L., Iwayama, S., Iwaya, M., Takeuchi, T., Kamiyama, S., Miyake, H., & Akasaki, I. (2018). Growth of high-quality AlN and AlGaN films on sputtered AlN/sapphire templates via high-temperature annealing. *Physica Status Solidi (B)*, *255*(5), 1700506. https://doi.org/10.1002/pssb.201700506.

[50] Huang, J., Niu, M., Sun, M., Su, X., & Xu, K. (2019). Investigation of hydride vapor phase epitaxial growth of AlN on sputtered AlN buffer layers. *CrystEngComm*, *21*(14), 2431–2437. https://doi.org/10.1039/C8CE02192A.

[51] Ke, W.-C., Liang, Z.-Y., Tesfay, S. T., Chiang, C.-Y., Yang, C.-Y., Chang, K.-J., & Lin, J.-C. (2019). Epitaxial growth and characterization of GaN thin films on graphene/sapphire substrate by embedding a hybrid-AlN buffer layer. *Applied Surface Science*, *494*, 644–650. https://doi.org/10.1016/j.apsusc.2019.07.211.

[52] Ishimoto, S., Han, D.-P., Yamamoto, K., Mano, R., Kamiyama, S., Takeuchi, T., Iwaya, M., & Akasaki, I. (2019). Enhanced device performance of GaInN-based green light-emitting diode with sputtered AlN buffer layer. In *Applied Sciences* (Vol. 9, Issue 4). https://doi.org/10.3390/app9040788.

[53] Ishimoto, S., Han, D.-P., Yamamoto, K., Kamiyama, S., Takeuchi, T., Iwaya, M., & Akasaki, I. (2019). Improvement of emission efficiency with a sputtered AlN buffer layer in GaInN-based green light-emitting diodes. *Japanese Journal of Applied Physics*, *58*(SC), SC1040. https://doi.org/10.7567/1347-4065/ab079f.

[54] Ge, S., Zhang, B., & Yang, C. (2019). Characterization of Er-doped AlN films prepared by RF magnetron sputtering. *Surface and Coatings Technology*, *358*, 404–408. https://doi.org/10.1016/j.surfcoat.2018.11.050.

[55] Song, Y., Kawamura, F., Shimamura, K., Ohgaki, T., & Ohashi, N. (2020). Development of a flux-film-coated sputtering (FFC-sputtering) method for fabricating c-axis oriented AlN film. *AIP Advances*, *10*(11). https://doi.org/10.1063/5.0025736.

[56] Zeng, Y., Ning, J., Zhang, J., Jia, Y., Yan, C., Wang, B., & Wang, D. (2020). Raman analysis of E2 (high) and A1 (LO) phonon to the stress-free GaN grown on sputtered AlN/graphene buffer layer. In *Applied Sciences* (Vol. 10, Issue 24). https://doi.org/10.3390/app10248814.

[57] Feng, Q., Ai, Y., Liu, Z., Yu, Z., Yang, K., Dong, B., Guo, B., & Zhang, Y. (2020). Structural characterization of AlN (11-22) films prepared by sputtering and thermal annealing on m-plane sapphire substrates. *Superlattices and Microstructures*, *141*, 106493. https://doi.org/10.1016/j.spmi.2020.106493.

[58] Bakri, A. S., Nayan, N., Ahmad, M. K., Fhong, S. C., Sahdan, M. Z., Bakar, A. S. A., Majid, W. H. A., Tahan, M., & Raship, N. A. (2020). Fabrication of w-AlN thin films using tilted sputter target and unrotated substrate holder. *International Journal of Integrated Engineering*, *12*(4), 50–56. https://doi.org/10.30880/ijie.2020.12.04.005.

[59] Gu, W., Liu, Z., Guo, Y., Wang, X., Jia, X., Liu, X., Zeng, Y., Wang, J., Li, J., & Yan, J. (2020). Comprehensive study of crystalline AlN/sapphire templates after high-temperature annealing with various sputtering conditions. *Journal of Semiconductors*, *41*(12), 122802. https://doi.org/10.1088/1674-4926/41/12/122802.

[60] Li, D.-D., Chen, J.-J., Su, X.-J., Huang, J., Niu, M.-T., Xu, J.-T., & Xu, K. (2021). Preparation of AlN film grown on sputter-deposited and annealed AlN buffer layer via HVPE. *Chinese Physics B*, *30*(3), 36801. https://doi.org/10.1088/1674-1056/abd392.

[61] Uesugi, K., Shojiki, K., Xiao, S., Kuboya, S., & Miyake, H. (2021). Effect of the sputtering deposition conditions on the crystallinity of high-temperature annealed AlN films. In *Coatings* (Vol. 11, Issue 8). https://doi.org/10.3390/coatings11080956.

[62] Shojiki, K., Uesugi, K., Kuboya, S., Inamori, T., Kawabata, S., & Miyake, H. (2021). High-quality AlN template prepared by face-to-face annealing of sputtered AlN on sapphire. *Physica Status Solidi (B)*, *258*(2), 2000352. https://doi.org/10.1002/pssb.202000352.

[63] Peng, W., Zhou, Y., Xiang, G., Liu, Y., Zhang, J., Zhang, J., Huang, H., Mei, M., Wang, H., & Zhao, Y. (2022). Preparation of AlN thin film and the impacts of AlN buffer layer on the carrier transport properties of p-NiO/n-InN heterojunction by magnetron sputtering. *Materials Science in Semiconductor Processing*, *141*, 106417. https://doi.org/10.1016/j.mssp.2021.106417.

[64] Peng, X., Sun, J., Liu, H., Li, L., Wang, Q., Wu, L., Guo, W., Meng, F., Chen, L., & Huang, F. (2022). Structural and optical properties of AlN sputtering deposited on sapphire substrates with various orientations. *Journal of Semiconductors*, *43*(2), 22801. https://doi.org/10.1088/1674-4926/43/2/022801.

[65] Ueoka, Y., Suemoto, Y., Kiuchi, M., Takahashi, T., Shimizu, M., & Mesuda, M. (2023). Fabrication and characterization of a high-electron-mobility transistor using a sputtering buffer layer on a Si substrate. *Journal of Crystal Growth*, *616*, 127259. https://doi.org/10.1016/j.jcrysgro.2023.127259.

[66] Liu, W.-S., Wu, S.-H., Balaji, G., Huang, L.-C., Chi, C.-K., & Kuo, H.-C. (2024). Optimization of high-quality gallium nitride thin films deposited on silicon substrates with an aluminum nitride buffer layer through radio-frequency magnetron sputtering. *Vacuum*, *227*, 113352. https://doi.org/10.1016/j.vacuum.2024.113352.

[67] Azman, Z., Nayan, N., Nazri, M. K. S. S., Bakar, A. S. A., Ali, R. A. M., Mohkhter, F., Sahari, N., & Hussin, M. R. M. (2024). Investigating Crystallography and Thickness Distribution of Aluminium Nitride Thin Films Prepared by Magnetron Sputtering on Silicon Wafer. *2024 IEEE 40th International Electronics Manufacturing Technology (IEMT)*, 1–5. https://doi.org/10.1109/IEMT61324.2024.10875098.